Materials Chemistry and Physics 198 (2017) 317–323

Contents lists available at ScienceDirect

Materials Chemistry and Physics

journal homepage: www.elsevier.com/locate/matchemphys

Phase stability in $MoTe_2$ prepared by low temperature Mo tellurization using close space isothermal Te annealing

E. Sánchez-Montejo [a, b], G. Santana [c], A. Domínguez [c], L. Huerta [c], L. Hamui [d, e], M. López-López [d], H. Limborço [f], F.M. Matinaga [f], M.I.N. da Silva [f], A.G. de Oliveira [f], J.C. González [f], O. de Melo [a, *]

[a] Physics Faculty, University of Havana, 10400, La Habana, Cuba
[b] Facultad de Ciencias Pedagógicas, Universidad de la Isla de la Juventud Jesús Montané Oropesa, La Demajagua, 27400, Isla de la Juventud, Cuba
[c] Instituto de Investigación en Materiales, Universidad Nacional Autónoma de México, Cd. Universitaria, A.P. 70-360, Coyoacán, 04510, México D. F., México
[d] Departamento de Física, Centro de Investigación y de Estudios Avanzados del IPN, Apartado Postal 14-740, México D. F., 07000, Mexico
[e] Facultad de Ingeniería, Universidad Anáhuac, Av. Universidad Anáhuac 46, Col. Lomas Anáhuac, Huixquilucan, Estado de México, C.P. 52786, Mexico
[f] Departamento de Fisica, Universidade Federal de Minas Gerais, Belo Horizonte, MG, 30123-970, Brazil

HIGHLIGHTS

- Isothermal close space annealing is used for tellurization of MoO_x films.
- Relatively low temperature of 500 °C was employed.
- Mixed 1T′/2H phases were obtained for small tellurization times.
- Highly oriented pure 2H phase is obtained for large tellurization times.
- Te/Mo chemical shifts between 1T′and 2H phase around 0.38/0.27 eV were found.

GRAPHICAL ABSTRACT

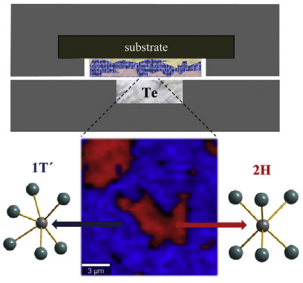

ARTICLE INFO

Article history:
Received 31 January 2017
Received in revised form
28 April 2017
Accepted 11 June 2017
Available online 12 June 2017

Keywords:
2D materials
Transition metals dichalcogenides
$MoTe_2$
Phase stability

ABSTRACT

In this work, we used isothermal close space (ICS) Te annealings in pure H_2 atmosphere for the tellurization of Mo oxide thin films. Differently to previous open tube tellurization annealings, ICS is expected to provide a higher Te vapor pressure because the chamber containing the Te source and the substrate is very small and semi-closed. Then, we used a relatively low temperature of 500 °C at which, according to the phase diagram, 2H phase should be stable. However, we observed that, in all cases, Mo oxide initially transformed to 1T′ before reaching the equilibrium 2H phase. Highly oriented $MoTe_2$ films with the [001] direction perpendicular to the surface were obtained in all samples. On the other hand, according our X-ray photoelectron spectroscopy measurements, we report shifts of 0.38/0.27 eV in the 3d emission of Te/Mo between the two different phases which probably have a chemical origin.

1. Introduction

Transition metal dichalcogenides (TMDs) are novel layered materials with formula MX_2 in which M stands for a transition metal (Mo, W, Nb, Re, etc.) and X for a chalcogen element (S, Se, Te).

* Corresponding author.
E-mail address: omelo@fisica.uh.cu (O. de Melo).

http://dx.doi.org/10.1016/j.matchemphys.2017.06.031
0254-0584/

Like graphene, they have a bidimensional (2D) nature with their basic element comprised of a hexagonally packed monolayer of the transition metal interleaved between two monolayers of the chalcogen element. Not having dangling bonds, interactions between these triple layers occur through weak Van der Waals bonds; hence, their laminar structure. Recently, they have received much interest from the scientific community [1,2] for numerous reasons. For example, opposite to graphene, some TMDs present a finite band gap which has been measured or predicted to range between 0.7 (WTe_2) and 2 eV (WS_2) [3,4]. This makes them compatible with the semiconductor industry [5]; in particular, they are very promising as a channel material in field effect transistors for logic circuits [6,7]. On the other hand, new phenomena associated with the low dimensionality, such as mechanical flexibility and chemical stability, make them promising materials for a wide range of applications.

$MoTe_2$, like other TMD materials, can exist in two distinct stable modifications: hexagonal (2H) and distorted octahedral (1T′) structure [8]. 2H-$MoTe_2$ has semiconducting properties with an energy band gap of 1.1 eV (for 1 ML sheet) [9], corresponding to the infrared region of the electromagnetic spectrum. The strong spin-orbit coupling in $MoTe_2$, due to the high value of Te atomic mass, makes it potentially useful for interesting new applications as valleytronics, spintronics, and quantum spin Hall Effect devices [10–12]. In contrast, 1T′modification presents a semi-metallic behavior and, as it was demonstrated very recently, it hosts an exotic Weyl state [13]. For these reasons, the control of the preparation conditions for obtaining one particular phase is a very important task in $MoTe_2$. However, conditions for the stability of these phases in this material are still a matter of discussion, as it will be described below.

Several approaches have been used for the preparation of TMDs [2,14]. In the case of $MoTe_2$, small area but good quality material consisting of few monolayers has been obtained by exfoliation of bulk single crystals [7,15] or by chemical vapor deposition [16]. Besides, tellurization of Mo or Mo oxide films has been used for the preparation of large area $MoTe_2$ films [17,18] of both 1T′ and 2H phases using an open tube Te annealing. In Ref. [17] a two zone furnace has been used to differentiate the cooling and/or heating step of both Te source and substrate. The authors used a tellurization temperature of 650 °C and found that well oriented 2H-$MoTe_2$ were obtained with slow tellurization rates and large tellurization time. They ascribe this behavior to the fact that, on the fast tellurization process, Mo crystallizes before the Te annealing and this leads to the formation of randomly oriented $MoTe_2$. In Ref. [18] the Te source and substrate are heated (and cooled) simultaneously but Mo precursor was previously oxidized. The authors concluded that, probably, 2H-$MoTe_2$ phase prevailed when the precursor oxide was MoO_3, while, for pure Mo or MoO_x (with $x < 3$) precursor, 1T′ phase predominates. They used a tellurization temperature of 700 °C. On the other hand, while some authors propose that the 2H → 1T′phase transition is reversible [7,14] others have demonstrated that it is not the case [19] and 2H phase never transforms to 1T′ at high temperature. Also, a mechanical route to induce the phase transition has been explored: tensile strain of 2H phase should stabilize the 1T′phase [20,21].

In this work, we investigated the synthesis of $MoTe_2$ through Mo tellurization using isothermal close space (ICS) annealing in pure H_2 atmosphere. With this simple procedure 2H and 1T′ $MoTe_2$ were obtained at a relatively low annealing temperature of 500 °C even if at this temperature one would expect that 2H-$MoTe_2$ should be stable for any Te/Mo stoichiometry [7,22].

X-ray diffraction (XRD) patterns and Raman spectra were used to identify the structure of the different samples while scanning electron microscopy (SEM), energy dispersive (EDS) and x-rays photoelectron (XPS) spectroscopies allowed to study morphology, chemical composition, and binding energies of the different species. We observed that, in our conditions, the degree of tellurization was the only factor influencing the stability of one or the other phase of $MoTe_2$. Small thickness of the Mo precursor and large tellurization times induced the formation of 2H phase despite differences in heating or cooling procedures. Our films are highly oriented with the [001] direction perpendicular to the surface. In contrast, partially tellurized Mo foils presented a random orientation of $MoTe_2$ crystals at the same conditions. A slight difference in the position of the XPS peaks is observed for the two different phases, probably due to a chemical shift between the 2H and 1T′phases.

2. Experimental methods

For tellurization experiments, Mo precursor films with nominal thickness of 15 and 50 nm were deposited using a DC Cressington Sputter Coater system equipped with a quartz balance. To promote the formation of Mo oxide, sputter chamber was evacuated at a low vacuum of 10^{-2} mbar. Then, Ar was introduced into the chamber; its pressure was set to 0.1 mbar and the current was adjusted to 40 mA. Previous to the Mo sputtering, 1 × 1 cm^2 Si (100) substrates were degreased with an organic solvent, cleaned with standard solution "p," H_2O:HNO_3:HF (100:10:1) and finally, rinsed with abundant water and isopropyl alcohol.

ICS Te annealings were carried out in a semi-closed boron nitride crucible placed inside a quartz reactor with a plate-shaped temperature profile which was fed with a 4 cm^3/s flow of H2 (purity: 99.9999%) provided by a hydrogen generator Packard 9200. Details of the boron nitride crucible are shown in Fig. 1. The upper part is movable from outside by means of a rod which is fed through the lateral cap of the reactor. The lower part has a bin, which is filled with a small amount of Te (99.9999% provided by GOODFELLOW). This type of crucible allows selecting the starting (or ending) time of the substrate exposure to the source and also to perform the heating (or cooling) process with the substrate exposed or not to the Te source. Distance between source and substrate (both at the same temperature) was five millimeters; this is the typical isothermal close space vapor transport geometry. In such semi-closed system, the Te vapors will not flow freely along the quartz reactor but are rather concentrated in the small growth compartment; then, one can expect that the vapor pressure of Te will be nearly equal to the equilibrium vapor pressure at the

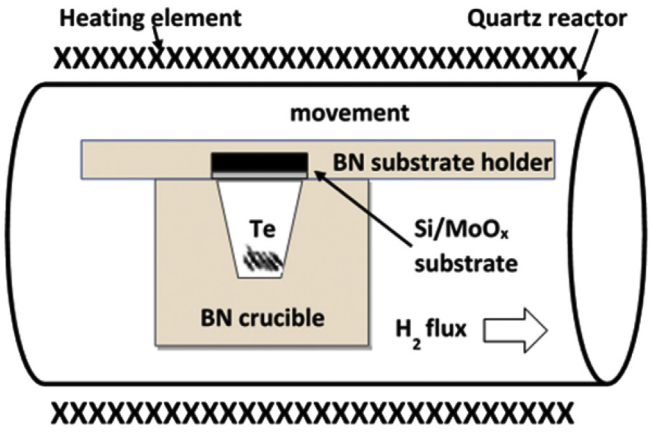

Fig. 1. Diagram of the semi-closed boron nitride crucible used for the isothermal Te annealings. The upper part is movable from outside of the quartz reactor (not shown) to permit heating or cooling steps with the substrate being exposed or not to the Te source.

temperature of the annealing and tellurization should be more efficient than in an open tube process in which Te vapor is more diluted in the carrier gas. In this conditions, one would expect that a lower temperature for tellurization annealing could be used.

In this conditions, one would expect that a lower temperature for tellurization annealing could be used. Using pure H_2 (instead of diluted H_2 in Ar of N_2) is supposed to enhance the efficiency of the tellurization as well.

To evaluate the rate of the process as well as the influence of the preparation conditions in the stability of the two different phases, tellurization times of 30 and 60 min were used. Table 1 resumes the growth conditions, and the resulting phases of the samples studied in this work.

The crystalline structure of the samples was inspected by XRD in coplanar geometry carried out on a PANalytical EMPYREAN diffractometer using the Cu-Kα 1.540598 Å line. SEM images were taken in a Jeol JSM-7600F and EDS spectra with an Oxford INCA X-ACT. The structural properties of the samples were also investigated by μ-Raman spectroscopy. The measurements were carried out at room temperature on a Jobin-Yvon T-64000 spectrometer in the triple monochromator backscattering configuration using the 100× (N. A. 0.9) magnifying lens of an Olympus BX-51 microscope and a liquid nitrogen cooled charge coupled device (CCD) detector. The excitation was performed with the 532 nm line of a linearly polarized Verdi™ Ti: Sapphire laser, with a spot size of approximately 1 μm and excitation power of 1 mW to avoid heating damages. For Raman maps of the films, we used a Witec Alpha300 RA confocal micro-Raman spectrometer equipped with a He–Ne laser (633 nm) as excitation source. A low incident power (~5 mW) was selected in order to avoid any beam-induced structural changes during measurements; an area of ~15 × 15 μm was scanned during the measurement. In order to get the colored pattern map, the peaks of E^1_{2g} and A_g from 2H and 1T′phases, respectively, were selected and overlapped. The topography and surface profilometry was obtained from the confocal Raman measurements without contact.

X-ray photoelectron spectroscopy analyses were performed in an ultra-high vacuum (UHV) Scanning XPS microprobe PHI 5000 VersaProbe II system, with an Al K_α X-ray source ($h\nu = 1486.6$ eV), and a MCD analyzer. Some measurements were made on previously eroded samples in which the surface was etched for 3 min with 1 kV Ar^+ ions at 55.6 nA mm^{-2}. The spectra were obtained at 45° to the normal surface in the constant pass energy mode (CAE), $E_0 = 100$ and 10 eV for survey and high-resolution narrow scan, respectively. The peak positions were referenced to the background silver $3d_{5/2}$ photopeak at 368:20 eV, having a FWHM of 0.56 eV, and C 1s hydrocarbon groups at 285.00 eV, Au $4f_{7/2}$ en 84.00 eV central peak core level position.

3. Results

Sputtered Mo films were found to be completely oxidized before tellurization experiments. This has been verified by noting systematically a larger film thickness value with respect to the nominal Mo thickness in a factor between 2 and 3 after sputtering process. Taking into account the molar masses of Mo, MoO_2 and MoO_3 (95.94, 127.92 and 143.96 g/mol) and the respective densities (10.28, 6.47 and 4.69 g/cm^3) a simple calculation provides the relation between the thickness of the formed oxide and that of the precursor Mo film in the case the oxidation occurred when the Mo film was exposed to air. Values of this relation are 2.11 and 3.28 for the formation of MoO_2 and MoO_3, respectively, the two best-known molybdenum oxides. Smaller, but same order values, can be obtained if the Mo was oxidized during sputtering deposition using the residual oxygen in the chamber. These values agree quite well with the observed thickness increments. Moreover, in Fig. 2 we present SEM images of the surface (a, b) at two different magnifications of a Mo oxide film formed with a sputtered Mo film of 50 nm. In Fig. 2c the diffractogram for the same sample measured in θ-2θ configuration showed a wide band due to amorphous or nanocrystalline Mo oxide.

Fig. 3a) presents x-rays diffractograms for samples from Table 1. Near to $2\theta = 33°$ a peak corresponding to the (002) crystalline plane of Si is observed. As can be seen in the figure, samples exposed to the Te source during the heating or cooling step of the annealing process, presents also a peak at around $2\theta = 27.5°$ that correspond with the (101) crystalline plane of Te which is its most intense peak according to the Joint Committee on powder diffraction standards (JCPDS) reference No. 00-004-0554. The rest of the peaks corresponds to $MoTe_2$ oriented with the [001] direction normal to the surface.

In samples A-D, $MoTe_2$ peaks present a doublet structure characteristic of the mix of the two phases. Fig. 3b) shows a narrow 2θ range around the (004) diffraction peak where it can be observed that two components are present at 25.45 and 25.84°, respectively. As it is well known in the literature [19], these components can be ascribed to the 2H and 1T′ phases of $MoTe_2$. Sample E, tellurized for 60 min and having a small thickness of 15 nm, presented only the peak at 25.45°. Diffractograms of other 15 nm samples tellurized for 60 min confirmed the above behavior, as shown in supplementary material S1. Also in S1, a diffractogram and a SEM image of a partially tellurized Mo foil are shown. The diffractogram revealed

Table 1
Growth condition of samples studied in this paper. All samples were grown at 500 °C.

Sample	Annealing time (min)	Nominal sputtered Mo thickness (nm)	Exposition to the Te source during heating/cooling	Main observed phase
A	30	50	Not exposed/exposed	1T′
B	30	50	Not exposed/exposed	1T′
C	60	50	Not exposed/exposed	2H
D	60	50	Not exposed/not exposed	2H
E	60	15	Not exposed/not exposed	Pure 2H

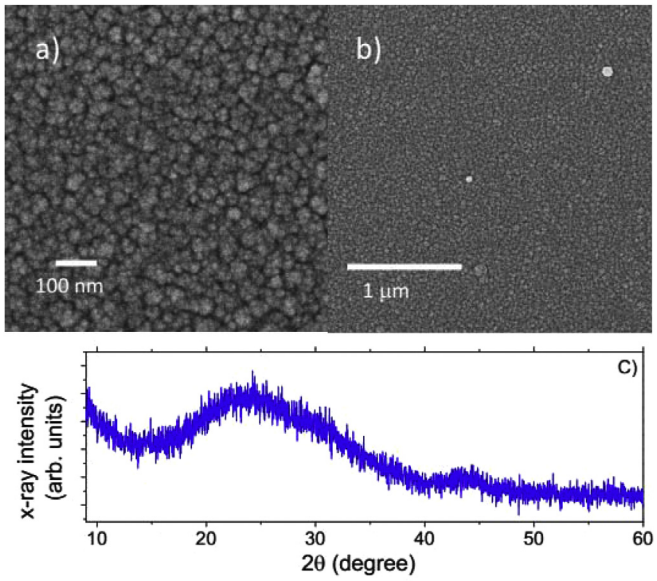

Fig. 2. a, b) SEM images of Mo oxide sputtered samples used for tellurization experiments at two different magnifications; c) θ-2θ diffractogram for the same sample.

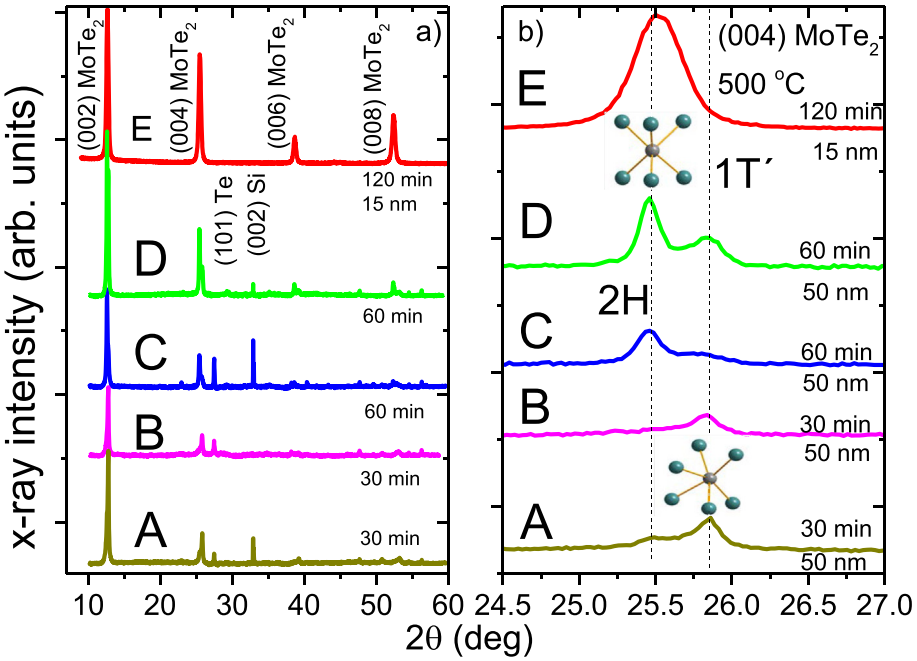

Fig. 3. a) X-rays diffractograms for samples studied in this paper; b) Part of the diffractograms in a narrow 2θ region around the 004-diffraction peak, showing the presence of both 2H and 1T′components of the peak. Schematic diagrams of 2H and 1T′cells (Te atoms in green and Mo atoms in gray) are inserted in b). (For interpretation of the references to colour in this figure legend, the reader is referred to the web version of this article.)

that the preferential orientation along [001] direction observed in the thin films was not present in this case.

It is well known that Raman spectroscopy is a helpful tool to identify the different phases in TMDs and particularly in $MoTe_2$ [5,23]. Fig. 4 shows an optical microscopy (a) image and the corresponding Raman map (b) for sample D in which both phases are present. In the map, the intensities of the peaks E^1_{2g} (red region) and A_g (blue region) from 2H and 1T′phases, respectively, were

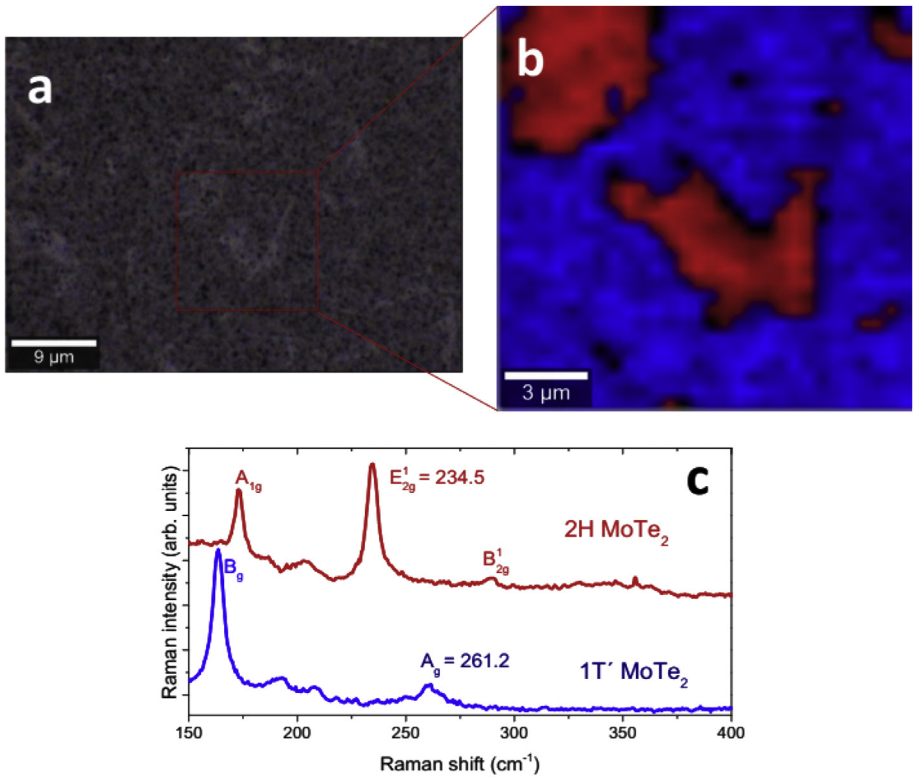

Fig. 4. a) Optical microscopy image of the region where the Raman map was made for sample D; b) Raman map of the intensities of the peaks E^1_{2g} (red region) and A_g(blue region) corresponding with the typical Raman spectra shown in (c). (For interpretation of the references to colour in this figure legend, the reader is referred to the web version of this article.)

scanned. Typical Raman spectra from the two different regions are shown in (c). As can be observed, both phases coexist for this sample in agreement with XRD results. Similar maps for other regions together with a topography one are shown in supplementary material S2. As previously noted in Ref. [17], the phases can also be differentiated by the contrast in the optical microscopy image. In fact, whitish and darker regions can be associated with 2H and 1T′phases, respectively. This is expected in view of the different electronic properties, and then refractive indexes of the two phases.

To investigate the origin of the Te peaks in the diffractograms, SEM/EDS analysis was carried out on sample C which shows a prominent peak related to this material. Small crystallites of pure Te were observed onto the surface of $MoTe_2$ as shown in Fig. 5a). For comparison, Fig. 5b) and c) shows the surface of samples D and E (heated and cooled without exposition to the source), where Te crystallites were not observed. It can be noted that the flaked morphology of the $MoTe_2$ is similar for the different samples in spite of the predominance of one phase or the other. Also, the Te/Mo height ratio in the EDS spectra (corresponding with the expected 1:2 Mo:Te stoichiometry) seems to be similar for the different samples, at least within the accuracy of the EDS measurement.

According to the above results, we suppose that the tellurization process occurs in the following way. Previous to the Te annealing, sputtered Mo oxidizes forming an amorphous or nanocrystalline MoO_{3-x}. During Te annealing, MoO_{3-x} starts to transform into crystalline 1T′ $MoTe_2$ consuming the oxide. However, before all the oxide is consumed, 1T′ $MoTe_2$ itself transforms to 2H phase and islands of this phase start to appear on the surface of the layer. With further tellurization, a pure 2H phase sample is obtained. According to this proposal, with the procedure followed in the present work and the low temperature annealing, 1T′ is a required transition phase from the oxide to the 2H phase. A scheme of this process is shown in Fig. 6. This behavior could be explained taking into account the phase stability dependence on strain [20,21]. At the beginning of the conversion of Mo oxide to $MoTe_2$, small islands of $MoTe_2$ are surrounded by the Mo oxide matrix; consequently, the $MoTe_2$ is highly strained. With the increase of the volume fraction of the 1T′ phase (increasing tellurization time) the strain is partially or totally relaxed and it transforms to the 2H phase.

Fig. 7 shows the XPS results for $MoTe_2$ samples. In a) typical low resolution survey spectra (in this case the spectrum corresponds to sample E, but the other samples showed identical features) without and with surface erosion are shown. The regions of Mo and Te lines in the sample without surface erosion show additional peaks that correspond to the oxide chemical states of both elements. In this spectrum, a peak corresponding with the O 1s line is also observed. The additional peaks of Te and Mo lines, as well as the O 1s line, disappear after surface erosion process which indicates the superficial character of the oxides. Also in the figure, high resolution spectra for samples A-E in the regions corresponding to Te 3d (b) and Mo 3d (c) core levels are presented (peaks corresponding to both $MoTe_2$ and superficial Mo and Te oxides are observed since the spectra were taken from samples that were not previously eroded). It is interesting to note that both, Mo and Te 3d doublets corresponding to $MoTe_2$ shifted to higher energies for samples richer in 2H phase with respect to the samples rich in 1T′phase. At the same time, peaks corresponding to the oxides approximately remain at the same energies. The shifts can be better observed in Fig. 7 d) and e) in which normalized $3d_{5/2}$ peaks are displayed in a narrow energy range. For samples A and E, with peaks located at extreme positions, the shift of Te/Mo peaks was around 0.38/0.27 eV. Very probably these peak position variations are due to a chemical shift between the two respective phases. An alternative description of the shift as due to different charging of 2H and 1T′phase during XPS measurements, but it can be discarded because in that case, oxides

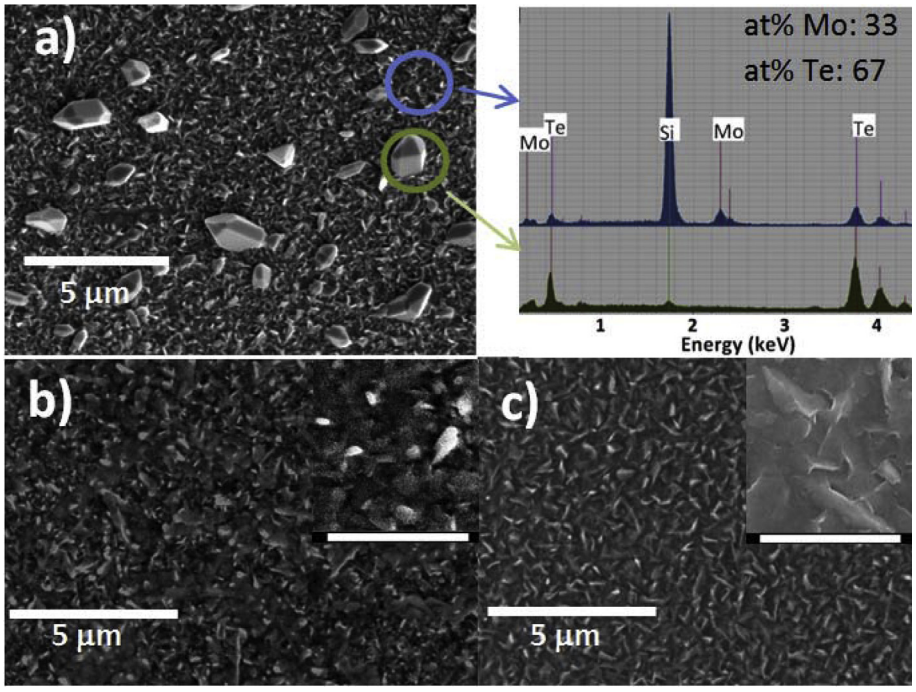

Fig. 5. a) SEM image of a characteristic region of the surface of sample C showing small crystals of pure Te onto the surface of $MoTe_2$ as verified by EDS spectra. The quantitative analysis of the spectrum of the $MoTe_2$ region provides atomic composition values of around 33 and 67% for Mo and Te elements, respectively, as expected according to the stoichiometry of the compound. b and c) For comparison, images of the surface of samples D and E are shown, Te crystallites were not observed in these samples. In the inset, higher magnification images with 1 μm scale bars are displayed.

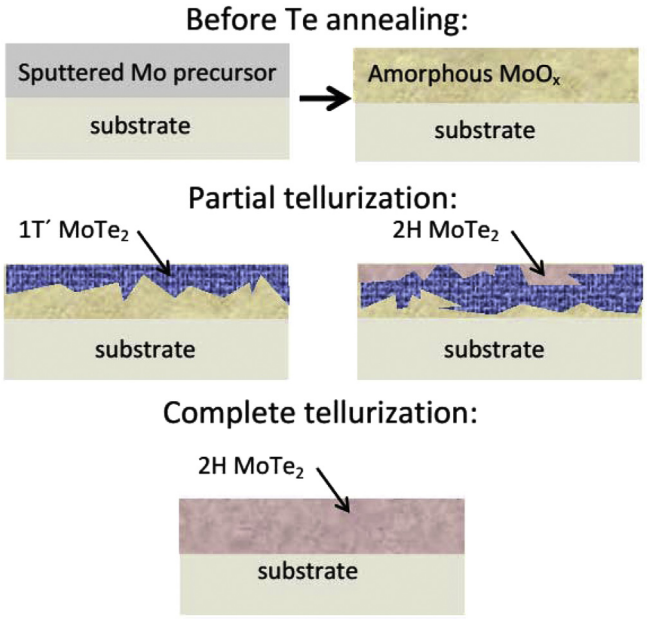

Fig. 6. Schematic of the tellurization process in our conditions of isothermal close space Te annealing.

peaks would be shifted as well.

These kinds of shifts between phases in TMDs were previously observed for MoS_2 samples [24] intercalated with Li. The authors of that paper observed shifts of 0.35 eV in both Mo 3d and S 2p doublets for small amounts of intercalated Li and shifts of 1.1 and 0.8 eV for Mo 3d and S 2p doublets, respectively, for higher amounts of intercalated Li. They ascribed the 0.35 eV shift to Fermi level displacements due to Li doping or the formation of an accumulation layer. On the other hand, they supposed that 1.1 and 0.8 eV shifts for Mo 3d and S 2p doublets were due to a transition from 2H to 1T phases of MoS_2 with the higher values of the peaks corresponding to the 2H phase. More recently, a chemical downshift of 0.9 eV was observed in the signal of Mo 3d, S 2s and S 2p for exfoliated MoS_2 annealed at different temperatures and was ascribed to a transition from 2H and 1T phases [25]. It could be expected that the shift observed in our samples for Te and Mo 3d doublets to higher energies as the proportion of 2H phase increases, has a similar nature of these previous observations for MoS_2 although the shift is smaller for our material. With well-calibrated XPS spectra, these shifts could be useful to discern about the presence of a phase or the other, beside Raman spectra, XRD patterns or optical contrast.

4. Conclusions

Highly oriented $MoTe_2$ films have been obtained using isothermal close space tellurium annealings. Samples of various thickness of sputtered Mo were annealed at 500 °C for different times. As we demonstrated, the predominance of one phase or the other depends only on the level of tellurization of the samples. For small levels of tellurization (smaller times, thicker samples) the 1T′phase was observed to predominate. For a high level of tellurization (larger times, smaller thickness) pure 2H phase was obtained. A mix of both phases was observed for intermediate tellurization. This is in spite of the fact that the temperature of tellurization was as low as 500 °C in which the phase diagrams of $MoTe_2$ predicts only the presence of 2H phase for any Te/Mo stoichiometry. A possible explanation for such behavior is that 1T′ phase is stabilizing as a consequence of strain developed during the conversion of Mo oxide to $MoTe_2$. According to the above results, the path for obtaining 2H $MoTe_2$ resides in performing the annealing at a temperature of 500 °C up to reaching the Te saturation of the film. We have demonstrated that with isothermal close space configuration it is possible to perform the annealing at such a low temperature. Finally, it was observed a chemically induced up-shift in the XPS peaks corresponding with the 3d levels of Mo and Te for samples with increasing amount of the 2H phase.

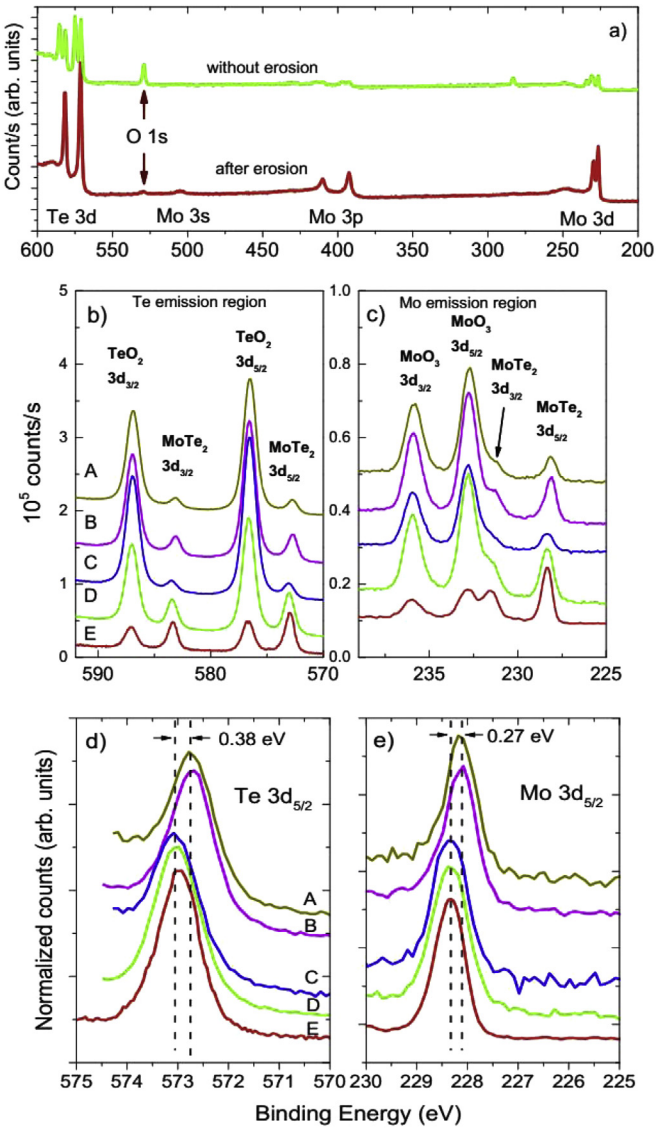

Fig. 7. a) Low resolution spectra for a typical sample with and without surface erosion. High resolution XPS spectra in the Te 3d (b) and Mo 3d (c) regions for samples A-E. An up-shift in the signal maximum for Mo and Te in the $MoTe_2$ peak is observed for samples in which 2H phase predominate, more evident in a narrow region of the spectra showing only de $3d_{5/2}$ peaks for both elements (d, e).

Acknowledgments

The authors acknowledge the CAPES (CAPES-INL 04/14, CAPES-PVE 88881.068066/2014-01), CNPq and FAPEMIG funding agencies for the financial support. Technical support of the Laboratory of Crystallography and the Center of Microscopy of the Universidade Federal of Minas Gerais is also acknowledged. Authors are indebted

with S. de Roux and E. Romero Ibarra for assistance.

Appendix A. Supplementary data

Supplementary data related to this article can be found at http://dx.doi.org/10.1016/j.matchemphys.2017.06.031.

References

[1] X. Duan, C. Wang, A. Pan, R. Yu, X. Duan, Chem. Soc. Rev. 44 (2015) 8859.
[2] L. Ruitao, J.A. Robinson, R.E. Schaak, D. Sun, Y. Sun, T.E. Mallouk, M. Terrones, Acc. Chem. Res. 48 (2015) 56.
[3] Q. Hua, K. Kalantar-Zadeh, A. Kis, J.N. Coleman, M.S. Strano, Nat. Nanotechnol. 7 (2012) 699.
[4] C. Gong, H. Zhang, W. Wang, L. Colombo, R.M. Wallace, K. Cho, Appl. Phys. Lett. 103 (2013) 053513.
[5] A.K. Geim, I.V. Grigorieva, Nature 999 (2013) 419.
[6] F. Schwierz, J. Pezoldt, R. Granzner, Nanoscale 7 (2015) 8261.
[7] B. Radisavljevic, A. Radenovic, J. Brivio, V. Giacometti, A. Kis, Nat. Nanotechnol. 6 (2011) 147.
[8] C. Ataca, H. Sahin, S. Ciraci, J. Phys. Chem. C 116 (2012) 8983.
[9] D.H. Keum, S. Cho, J.H. Kim, D.H. Choe, H.J. Sung, M. Kan, H. Kang, J.Y. Hwang, S.W. Kim, H. Yang, K.J. Chang, Y.H. Lee, Nat. Phys. 11 (2015) 482.
[10] D. Xiao, G.B. Liu, W. Feng, X. Xu, W. Yao, Phys. Rev. Lett. 108 (2012) 196802.
[11] X. Qian, J. Liu, L. Fu, J. Li, Science 346 (2014) 1344.
[12] N. Zibouche, P. Philipsen, A. Kuc, H. Thomas, Phys. Rev. B 90 (2014) 125440.
[13] L. Huang, T.M. McCormick, M. Ochi, Z. Zhao, M.T. Suzuki, R. Arita, Y. Wu, D. Mou, H. Cao, J. Yan, Nat. Mater. 15 (2016) 1155.
[14] Y. Shi, H. Li, L.J. Li, Chem. Soc. Rev. 44 (2015) 2744.
[15] C. Ruppert, O.B. Aslan, T.F. Heinz, Nano Lett. 14 (2014) 6231–6236.
[16] C.H. Naylor, W.M. Parkin, J. Ping, Z. Gao, Y.R. Zhou, Y. Kim, F. Streller, R.W. Carpick, A.M. Rappe, M. Drndić, Nano Lett. 16 (2016) 4297.
[17] J.C. Park, S.J. Yun, H. Kim, J.H. Park, S.H. Chae, S.J. An, J.G. Kim, S.M. Kim, K.K. Kim, Y.H. Lee, ACS Nano 9 (2015) 6548.
[18] L. Zhou, K. Xu, A. Zubair, A.D. Liao, W. Fang, F. Ouyang, Y.H. Lee, K. Ueno, R. Saito, T. Palacios, J. Kong, M.S. Dresselhaus, J. Am. Chem. Soc. 137 (2015) 11892.
[19] K. Ueno, K. Fukushima, Appl. Phys. Express 8 (2015) 095201.
[20] K.A.N. Duerloo, Y. Li, E.J. Reed, Nat. Commun. 5 (2015) 4214.
[21] H.H. Huang, X. Fan, D.J. Singh, H. Chen, Q. Jiang, W.T. Zheng, Phys. Chem. Chem. Phys. 18 (2016) 4086.
[22] L. Brewer, R. H. Lamoreaux, ASM Alloy Phase Diagram Database (ASM International, 2006) http://www1.asminternational.org/AsmEnterprise/APD.
[23] M. Kan, H.G. Nam, Y.H. Lee, Q. Sun, Phys. Chem. Chem. Phys. 17 (2015) 14866.
[24] C.A. Papageorgopoulos, W. Jaegermann, Surf. Sci. 338 (1995) 83.
[25] G. Eda, H. Yamaguchi, D. Voiry, T. Fujita, M. Chen, M. Chhowalla, Nano Lett. 11 (2011) 5111.